

**Actin organizations in single dendritic spines  
studied with two-photon photoactivation**

Naoki Honkura

DOCTOR OF PHILOSOPHY

Department of Physiological Sciences  
School of Life Science  
The Graduate University for Advanced Studies  
(SOKENDAI)

2005

## **CONTENTS**

	<b>Page</b>
<b>Summary</b>	<b>3</b>
<b>Introduction</b>	<b>4</b>
<b>Materials and Methods</b>	<b>6</b>
<b>Results</b>	<b>10</b>
<b>Discussion</b>	<b>18</b>
<b>Acknowledgement</b>	<b>24</b>
<b>References</b>	<b>25</b>
<b>Figures</b>	<b>30</b>

## **Abstract**

The major cytoskeleton of dendritic spines is filamentous actin (F-actin). Organizations of F-actin within individual spines, however, have not been elucidated. I have here investigated sub-spine actin organizations using two-photon photoactivation of PA-GFP fused with  $\beta$ -actin in rat CA1 pyramidal neurons in slice culture preparations. I found segregated and discontinuous organizations of two pools of F-actin, dynamic and stable pools, which turned over with time constants of 1.2 min and 17 min, respectively. The stable F-actin pool was localized at the base of spine head, often intruding into thick spine neck, while the dynamic pool occupied the rest of spine head. Fractions of the stable F-actin pool were greater in larger spines, therefore, the entire F-actin pool was more stable in larger spines. I succeeded in visualizing a retrograde flow of F-actin in the dynamic pool from the apex to the base of spine, and found that both the speeds (0.2-1.2  $\mu\text{m}/\text{min}$ ) and lengths (0.2-0.7  $\mu\text{m}$ ) of the F-actin flow were greater in spines with larger head volumes. Moreover, spine heads rapidly shrank when actin polymerization was blocked by latrunculin A, suggesting that the rate of actin polymerization in each spine actively and continuously determines the volume of spine head via the length of F-actin. Thus, I have revealed the sub-spine organizations of actin filaments that play key role in spine structures and diversity.

## Introduction

Dendritic spines are the major postsynaptic sites for excitatory synaptic inputs to the pyramidal neurons. They have a round head and a thinner neck structure, both of which are highly variable in their sizes (Harris and Stevens, 1989;Noguchi et al., 2005). Structural plasticity of single dendritic spines underlies long-term potentiation (LTP) of excitatory synaptic inputs (Matsuzaki et al., 2004;Hayashi and Majewska, 2005). It has also been clarified that plasticity and stability of spines are widely different among spine types (Matsuzaki et al., 2004;Holtmaat et al., 2005). It is well known that the major cytoskeleton of dendritic spines is filamentous actin (F-actin) (Matus et al., 1982), most of which turns over rapidly with a time constant of ~1 min (Star et al., 2002). In general, F-actin continuously undergoes treadmilling – polymerization with monomer actin (G-actin) at the barbed end and depolymerization at the pointed end. At the leading edge of cells, such as lamellipodia and axonal growth cones, actin filaments assemble at the edge, and induce a retrograde flow of actin into the cytosol (Pollard and Borisy, 2003;Zhang et al., 2003). Such peripheral actin networks are highly branched (Pollard and Borisy, 2003).

The organizations of actin in single spines have been difficult to study with conventional electron microscopic investigations, because actin binding proteins are so dense in spines that antibodies are often inaccessible to F-actin. In addition, individual spines have been too small for optical methods to directly visualize the dynamics of actin organizations. It has therefore been not clarified how actin organizations underlie spine head and neck structures, and how they

are diverse among distinct spines.

I have here applied two-photon photoactivation of PA-GFP (Patterson and Lippincott-Schwartz, 2002; Schneider et al., 2005) which was fused with  $\beta$ -actin to study actin organizations of single spines in slice culture preparations. PAGFP-actin could be rapidly photoactivated, and emitted bright fluorescence with two-photon excitation imaging. Using this approach, I have, for the first time, visualized actin organizations in spines and dendritic shafts. F-actin could be readily distinguished from G-actin, since G-actin quickly diffused out. I found two distinct F-actin pools, dynamic and stable pools, which were segregated in single spines, and which had variable contributions among distinct spines. I succeeded in visualizing a retrograde flow of actin in the dynamic pool, and revealed that both speeds and lengths of the actin flow were greater in larger spines, indicating that the rate of actin polymerization determined the volume of each spine head. Thus, I have revealed sub-spine actin-organizations which play an essential role in spine structures and their plasticity.

## **Materials and methods**

### **Preparations**

Hippocampal slices with a thickness of 350  $\mu\text{m}$  were prepared from 6- to 8-day-old Sprague-Dawley rats. Slices were mounted on 0.4- $\mu\text{m}$  culture inserts (Millipore, Billerica, MA, USA) and incubated at 35°C under 5%  $\text{CO}_2$  in medium comprising 50% MEM (Invitrogen, Carlsbad, CA, USA), 25% Hanks' balanced salt solution (Invitrogen), 25% horse serum (Nichirei, Tokyo, Japan), and 6.5 g  $\text{l}^{-1}$  glucose (Nacalai Tesque, Kyoto, Japan). After 8 to 10 days in vitro, slices were transfected, with the use of a Gene Gun system (PDS-1000; Bio-Rad, Hercules, CA, USA), with a vector containing two GFP constructs described below. Imaging experiments were performed three to seven days after transfection. Each culture insert was transferred to a recording chamber and superfused with a solution (ASCF) that contained 125 mM NaCl, 2.5 mM KCl, 2 mM  $\text{CaCl}_2$ , 1 mM  $\text{MgCl}_2$ , 1.25 mM  $\text{NaH}_2\text{PO}_4$ , 26 mM  $\text{NaHCO}_3$ , and 20 mM glucose and which was bubbled with 95%  $\text{O}_2$  and 5%  $\text{CO}_2$ . The second to third dendritic branches were mainly used for imaging experiments. All physiological experiments were performed at room temperature (23° to 25°C). The experiments were approved by the Animal Experiment Committee of the National Institute for Physiological Sciences.

### **Two-photon excitation imaging and photoactivation**

Two-photon imaging of dendritic spines was performed with an upright microscope (BX50WI; Olympus, Tokyo, Japan) equipped with a water immersion

objective lens (LUMFL60xW, numerical aperture of 1.1) and with FV1000 laser scanning microscope system (FV1000, Olympus). Two mode-locked femtosecond-pulse Ti:sapphire lasers (MaiTai, Spectra Physics, Mountain View, CA; Chameleon, Coherent, Santa Clara, CA) set at wavelengths of 710 and 960 nm were connected to the laser-scanning microscope via two independent scan-heads, and were gated with two acoustico-optic modulators (AOM). I used mRFP, or DsRed2, for imaging of spine structures and PAGFP-actin, or Venus-actin, for imaging of actin dynamics. Fluorescence lights from PAGFP-actin (or Venus-actin) and mRFP (DsRed2) were acquired at 500-550 nm and 590-680 nm, respectively. There was a small cross-talk from mRFP to PAGFP channel by 1.5%, which were small and not subtracted for image and quantitative analyses. The point-spread function of the focal volume at 960 nm was estimated with the use of 0.1- $\mu\text{m}$  fluorescent beads as 0.36  $\mu\text{m}$  (FWHM) laterally and 1.6  $\mu\text{m}$  axially. For three-dimensional reconstruction, 81 xy-images separated by 0.05  $\mu\text{m}$  were stacked by summation of fluorescence values at each pixel. Two-photon photoactivation of PAGFP-actin was effected at 710 nm either at single point of image during a short interval of 1-10 ms or at a certain circular region compassing a dendritic spine for 10-50 ms using "tornado" scan options of FV1000. The power of the photoactivation laser was set in between 2.5 and 25 mW.

### **Estimation of spine-head volume**

Spine-head volume was estimated from the total fluorescence of the spine head in the z-stacked fluorescence images, which were calibrated with the use of the

most spherical large spine in the same dendritic field. In the stacked image of the large spine, the one-dimensional fluorescence profile crossing the center of the head,  $f(r)$ , was measured, and fitted by the following equation:

$$F(r,R) = \frac{A}{(2\pi)^{3/2} \sigma_x^2 \sigma_z} \iiint_{x^2+y^2+z^2 < R^2} dx dy dz \int dz' e^{-\left[\frac{(x-r)^2}{2\sigma_x^2} + \frac{y^2}{2\sigma_x^2} + \frac{(z-z')^2}{2\sigma_z^2}\right]}$$

where  $A$  represents the intensity at the center ( $r = 0$ ) of the unit sphere,  $R$  the radius of the spine head, and  $\sigma_x$  (0.17  $\mu\text{m}$ ) and  $\sigma_z$  (0.54  $\mu\text{m}$ ) the standard deviations of the Gaussian approximation of the focal volume of 2P excitation.

$F(r, R)$  was numerically obtained with Mathematica4 software (Wolfram Research, Champaign, Illinois) to find the value of  $2R$  that fits with full-width-at-half-maximal (FWHM) diameter of  $f(r)$ . The spine-head volume

was then estimated as  $\frac{4}{3}\pi R^3$ . This procedure established a coefficient

between spine fluorescence and its volume. Once this coefficient was obtained, it was applied to every spine in the same dendritic region.

### **Constructs of plasmids**

The human cytomegalovirus immediate early (CMVIE) promoter of pEGFP-C1 vector (Clontech, Palo Alto, CA) was replaced with CAG promoter at the NdeI and NheI sites by PCR-amplification using the forward primer 5'-AATGACGTATGTTCCCATAGTAACGCC-3' and the reverse primer 5'-CTAGCTAGCTCTTTGCCAAAATGATGAGACAGCACA-3' (pCAG-EGFP-C1). Then, EGFP region of pCAG-EGFP-C1 vector was replaced with PAGFP (a gift from Patterson GH., Lippincott-Schwartz J.) or Venus at NheI and BsrGI sites

(pCAG-PAGFP-C1 or pCAG-Venus-C1). The human  $\beta$ -actin sequence was inserted in pCAG-PAGFP-C1 plasmid at XhoI and BamHI sites (pCAG-PAGFP-actin) and pCAG-Venus-C1 plasmid at XhoI and BamHI sites (pCAG-Venus-actin). For constructing mRFP1 and DsRed2 vectors, either mRFP1 or DsRed2 (Clontech) was inserted into pCAG-EGFP-C1 vector by NheI and EcoRI site (pCAG-mRFP1 or pCAG-DsRed2 vectors).

## Results

### Quantification of G- and F-actin in the dendrites

I studied properties of actin in dendrites of CA1 pyramidal neurons transfected with PAGFP-actin and mRFP. I used mRFP for monitoring spine structures, since it homogenously stained the cytosol (Fig.1A), and since it has only a little spectral overlap with PAGFP. There was no abnormality in dendritic branches and spine structures compared with preparations stained only with GFP (Matsuzaki et al., 2001;Noguchi et al., 2005), indicating that expression of PAGFP-actin did not significantly alter dendritic and spine structures.

PAGFP-actin was fluorescent when excited at 710 nm even before photoactivation (Fig. 1B) (Schneider et al., 2005), with which I studied the distribution of actin in dendrites. I found that spines contained greater concentrations of actin as relative to dendritic shafts (Fig. 1A, B), consistent with previous works using immunohistochemistry (Matus et al., 1982). I estimated the concentrations of PAGFP-actin in spine head and dendritic shaft head by normalizing fluorescence of PAGFP-actin with that of mRFP. The concentrations thus obtained were about  $6.3 \pm 0.6$  (mean  $\pm$  SD,  $n = 6$ ) times greater in spine head than in dendritic shaft.

To identify a fraction of G-actin in the dendritic shaft, I photoactivated PAGFP-actin with an excitation wavelength of 710 nm at a single point in the dendrite shaft for 1 ms (Fig. 1D). Two-photon fluorescent images were acquired with a line scanning mode every 3 ms along the dendrite with an excitation wavelength of 960 nm, which selectively detected photoactivated

PAGFP-actin (Fig. 1C). Fluorescence activated at the focal point decayed with a time constant of about 5 ms (Fig. 1D-F), while about 30% of the fluorescence remained stable (Fig. 1E). Fluorescence rapidly spread laterally during the decay phase, indicating that the decay reflected diffusion of PAGFP-actin along dendritic shaft (Fig. 1G).

The spatial profile of the diffusion could be fitted with Gaussian functions whose variances were linearly increased from  $0.65 \mu\text{m}^2$  to  $1.24 \mu\text{m}^2$  in 10 ms (Fig. 1H). This predicts that the mean square displacement (MSD) of PAGFP-actin was  $0.6 \mu\text{m}^2$  ( $=1.24 - 0.65$ ) for 10 ms, indicating the diffusion constant of PAGFP-actin as  $30 \mu\text{m}^2/\text{s}$ , based on the equation,  $\text{MSD} = \sqrt{2Dt}$  (Crank, 1975), where  $D$  and  $t$  are the diffusion constant and the time after photoactivation. The value  $30 \mu\text{m}^2/\text{s}$  is consistent with that of molecule with a molecular weight of 70 kDa in the cytosol (Swaminathan et al., 1997).

The variances of PAGFP-actin fluorescence reached the peak at 100 ms (Fig. 1I), and then gradually reduced by the time when the decay of PAGFP-actin fluorescence became markedly slowed (Fig. 1F), indicating the presence of an immobile pool of PAGFP-actin. The remaining stable component must represent F-actin, because polymerization is only a known mechanism that immobilizes large amounts of actin (Pollard and Borisy, 2003). The fraction of F-actin within the total actin pool in dendritic shaft was thus estimated as 31% ( $\pm 3.3\%$ , SD,  $n = 7$ ), by extrapolating the slowly decaying component by a straight line (Fig. 1F). Thus, the major actin in the dendritic shaft was G-actin. Most F-actin in dendritic shaft disappeared within 3 min (data not shown).

In contrast, the major population of actin was F-actin in spines. I used

the line scanning mode across spine heads, and photoactivation was effected at the center of spine head for 50-500 ms (Fig. 2A,B). I found that only a small fraction ( $12\% \pm 5.7\%$ , SD,  $n = 7$ ) of activated PAGFP-actin rapidly decayed with time constants of about 100-400 ms (Fig. 2C), consistent with G-actin fractions estimated by photobleaching of GFP-actin in dissociated culture neurons (Star et al., 2002). A small contribution of the fast component did not allow us to perform precise kinetic analysis of the fast decay, but it was consistent with simple diffusion of G-actin through a spine neck. Indeed, the diffusion constant of PAGFP-actin of  $30 \mu\text{m}^2/\text{s}$  predicts the spine neck PAGFP-actin conductance of  $0.15 - 20 \mu\text{m}^3/\text{s}$  ( $g_N$ ) (Noguchi et al., 2005), which can empty spine head with a volume of  $0.1 \mu\text{m}^3$  ( $V_H$ ) with a time constant of  $5 - 670 \text{ ms}$  ( $= V_H/g_N$ ).

Concentrations of G-actin were similar in spine heads and dendritic shafts. If I express the concentration of total actin molecules in spine head as 1 spine unit (s.u.), concentrations of G-actin and individual actins in F-actin pool were 0.12 s.u. and 0.88 s.u., respectively in spines, while 0.11 s.u. (0.69/6.3) and 0.049 s.u. (0.31/6.3), respectively, in dendritic shaft (Fig. 2D). Thus, G-actin concentrations were similar in spine and dendritic shaft, although concentrations of actins in F-actin pool were 18 times greater in spine head relative to dendritic shaft. This result is consistent with the fact that phalloidin staining is most concentrated in the dendritic spines (Allison et al., 1998; Capani et al., 2001).

### **Dynamic and stable F-actin contents in spines**

I next investigated properties of F-actin in individual spines and their dependence on spine-head volumes. I first examined dynamics of F-actin in an

entire spine by photoactivation of PAGFP-actin in a circular region that encompassed a spine head (Fig. 3A). The duration of the regional photoactivation was short, 10-50 ms, relative to the decay of F-actin fluorescence of ~1 min (Fig. 3B,C). In order to study the fast time courses of F-actin turnover, I rapidly acquired two dimensional images of spines at the central plane of each spine repeatedly with an interval of 2-10 s without three dimensional imaging and reconstruction. For the two dimensional imaging, it was essential that spines did not significantly ( $< 0.2 \mu\text{m}$ ) translocate along z-axis during a recording period over 10 min. I confirmed the absence of the translocation by the stability of fluorescence images of mRFP (data not shown). The sufficient stability was achieved only in 30% of experiments.

I found that the decay of PAGFP-actin fluorescence occurred in two phases with time constants of 1.2 min ( $\pm 0.27$  min,  $n = 12$ ) and about 17 min, respectively (Fig. 3B,C), which I referred to as dynamic and stable pools, respectively. The fraction of the stable pool was obtained by double exponential fitting of the decay with amplitudes of  $F_d$  and  $F_s$ , and the stable fraction was obtained as  $F_s/(F_s+F_d)$ . I found that the fractions of the stable pool were proportional to spine-head volumes (Fig. 3D). The slow decay time constants were obtained as  $17 \pm 3$  min (mean  $\pm$  SD,  $n = 3$ ) in experiments where preparations were stable over 30 min (data not shown).

I also found that spine-head volumes tightly correlated with the total F-actin contents ( $F_s+F_d$ ) which was estimated by the fluorescence of PAGFP-actin immediately after photoactivation in spines (Fig. 3E). For this type of experiments, I need to use the same dendritic branches, since absolute

levels of expression of PAGFP-actin varied from cell to cell. The correlation coefficient was obtained as 0.95 in 3 dendrites. The fact that both the total F-actin content ( $F_S+F_D$ ) and the fraction of the stable F-actin pool ( $F_S/(F_S+F_D)$ ) were proportional to spine-head volumes indicates that the stable F-actin content ( $F_S$ ) must be proportional to the second power of spine-head volumes. I directly confirmed this fact by measuring the both parameters from the same dendrites (Fig. 3F), although the stable kinetic measurements were successful in only 2-6 spines in a dendrite for 5 min. Double logarithmic plots confirmed that the stable F-actin content was dependent on the second power of spine-head volumes (Fig. 3F).

### **Spatial distributions of dynamic and stable F-actin pools**

The stable pool was localized at the base of spine, since F-actin signal remained selectively at the base of spines at 5 min after whole-spine photoactivation (Fig. 4A,B). The spatial distribution of the dynamic pool (Fig. 4C, c1) was estimated by subtracting the scaled image of the stable pool (Fig. 4C, c2) from the image immediately after photoactivation (Fig. 4B, b1). Thus, the two pools of F-actin were mostly segregated within a spine (Fig. 4C,D), although there were some overlaps (Fig. 4E).

F-actin dynamics was further studied with photoactivation of PAGFP-actin at a single point in a spine. I found that the turnover rate of F-actin was as fast as the dynamic pool when photoactivation was induced at the apex of spines (Fig. 5A,B), consistent with whole-spine activation (Fig. 4). I have further found a flow of PAGFP-actin fluorescence from the apex to the base

of spines when spines have sufficient dimension for selective spatial activation (Fig. 5D,E), as analyzed in detail below (see Fig. 7). In contrast, when I photoactivated at the base of spine, the majority of fluorescence remained at the site of activation (Fig. 5C,F), consistent with the localization of stable F-actin studied with whole-spine photoactivation (Fig. 4). I have failed to detect any flow of actin in the stable pool (data not shown).

Importantly, the stable and dynamic pools were little activated by the apical and basal photoactivation, respectively, if any (Fig. 5B,C). This suggests that the dynamic and stable pools were essentially discontinuous, and actins in one pool did not directly flow into the other. Slight activations of the other pools, which are seen in fluorescent profiles (Fig. 5E,F), could be ascribed to unavoidable spreads of photoactivation due to the lateral spatial resolution of our microscope of 0.36  $\mu\text{m}$  in FWHM diameter.

Point photoactivation of PAGFP-actin at the base of spine also revealed that the stable pool often (38%,  $n = 25$ ) intruded into spine neck (Fig. 6A,B). It appeared that the stable pool intruded into spine neck always and only when the necks were thick (Fig. 6B, b3-b5), but not when they were thin (Fig. 6B, b1, b2). Moreover, the stable pool invaded into the thick region of a spine neck (Fig. 6Bb1). Thus, the stable F-actin pool likely contributes in the formation of thick necks. It was also confirmed by point activation at the base of the spine that the fraction of the stable F-actin pool was greater in spines with larger heads (Fig. 6C), as well as confirmed the abundance of stable F-actin in large spines (Fig. 3D).

The flow of F-actin fluorescence in the dynamic pool was quantified by

the mean x-positions of PAGFP-actin fluorescence (Fig. 7A,B) in the fluorescence profiles along x-axis using Gaussian fitting (Fig. 5B and E). The speeds of the actin flow were obtained from the maximal slope of the plot shown in Fig.7A and B as 0.2-1.2  $\mu\text{m}/\text{min}$ , and were significantly greater ( $P < 0.01$ ,  $n = 9$ ) in larger spines (Fig. 7C). The lengths of the actin flow were obtained from the maximal value of the mean x-positions from the original position as 0.2-0.7  $\mu\text{m}$ , which were also greater for larger spines ( $P < 0.05$ ,  $n = 9$ ) (Fig. 7A,B and D). Thus, both the speeds and lengths of the actin flow were greater in larger spines. This was corroborated with the fact that the turnover rates of dynamic F-actin were not significantly different among spines ( $P = 0.8$ ,  $n = 12$ ) (Fig. 7E,F), because the effects of head volumes on the speeds and lengths of the actin flow cancelled out for the turnover rates. Thus, even though the turnover rates were similar among spines, the rates of actin polymerization were greater in spines with larger heads, and likely affected the volumes of spine heads via the lengths of F-actin.

### **Shrinkage of spine heads via blockade of actin polymerization**

To test whether actin polymerization directly determines spine-head volumes, I artificially halted the treadmilling of F-actin by an inhibitor of actin polymerization, latrunculin A (Lat A), in slice culture preparations transfected with Venus-actin and mRFP1 (or DsRed2). I found that Lat A (10  $\mu\text{M}$ ) treatment reduced both actin concentrations and spine-head volumes (Fig. 8A) within 10 min after application (Fig. 8B) ( $n = 4$ ). Shrinkage was induced in all spines examined irrespective of spine-head volumes (Fig. 8C). Thus, continuous polymerization

of F-actin was necessary to maintain spine structures in slice preparations.

## Discussion

Using two-photon photo-activation of PAGFP-actin, I have, for the first time, revealed segregated and discontinuous organizations of two F-actin pools in single dendritic spines. I have directly visualized the direction of actin filaments in single spines, consistent with the prediction made by early electron-microscopic investigations (Fifkova, 1985). I estimated the speeds and lengths of the actin flow in the dynamic F-actin pool, and found that spine-head structures were dynamically determined by the rate of actin polymerization. I also found that F-actin was more stable in larger spines.

### **Rapid diffusion of G-actin in dendrites**

I have revealed that G-actin rapidly diffuse along dendritic shaft consistent with free diffusion of a protein with a molecular weight of 70 kDa (Swaminathan et al., 1997). The concentrations of G-actin were similarly estimated in dendritic shaft and spines, suggesting that G-actin is almost equilibrated in the dendrites, despite a diffusion barrier possibly imposed by spine neck (Noguchi et al., 2005). In fact, the turn-over time constant of F-actin was at most 1.2 min, which was far longer relative to the time constant of G-actin diffusion from spine of 0.1-0.4 s. Thus, spine necks cannot limit the rate of F-actin polymerization by regulating supply of G-actin. The situation makes a clear contrast with  $\text{Ca}^{2+}$  signaling in spines, where spine necks play determinant role in the signaling process, because diffusion of  $\text{Ca}^{2+}$  across spine necks is slower than the other  $\text{Ca}^{2+}$  signaling mechanisms (Noguchi et al., 2005).

### **Dynamic F-actin pool in spines**

I have demonstrated that the mean length of F-actin flow (0.2-0.7  $\mu\text{m}$ ) in each spine nearly (~70%) reached the spine-head diameters (0.3-1  $\mu\text{m}$ ), suggesting that a significant population of individual actin filaments spanned almost the entire spine-head structures. Moreover, the speeds of the actin flow were faster in larger spines, indicating that the rates of actin polymerization were greater in larger spines. Since actin polymerization can generate a propulsive force towards the membrane (Mogilner and Oster, 1996), the greater rates of actin polymerization in larger spines should generate stronger forces for expansion of spine heads, given that actin filaments spanned the entire spine heads. Thus, the greater expansive forces of larger spines may be the major reason for larger spine heads. Indeed, a blocker of actin polymerization (Lat A) induced rapid and marked shrinkage of spines. These indicate that the shapes of spines are actively and continuously maintained by the precise balance between the expansive force of a spine and the mechanical stresses of tissues surrounding the spine. Consistently, Lat A was reported to induce shrinkage of spines more slowly and to a less degree in dissociated culture preparations (Allison et al., 1998; Korkotian and Segal, 2001; Okamura et al., 2004), where spines were not entirely surrounded by tissues.

It has been known that enzymatic activities for actin polymerization were present in postsynaptic density (PSD) (Hering and Sheng, 2001). The size of PSD can thus be translated into the volume of spine head, consistent with the finding that the two variables show a tight correlation in electron microscopic

analysis (Harris and Stevens, 1989). These data are also consistent with the observations that spine heads are enlarged by overexpression of many scaffolding proteins in PSD (Hering and Sheng, 2001), such as PSD95 (El-Husseini et al., 2000), SPAR (Pak et al., 2001), Shank and Homer (Sala et al., 2001). Spine heads are also enlarged by Eph-B receptors (Irie and Yamaguchi, 2002) and syndecan-2 (Ethell et al., 2001) which are also present in spines and induce actin polymerization. The speeds of actin flow in the dynamic F-actin pool are similar to retrograde flows of peripheral actin in growth cones of *Aplysia* (Zhang et al., 2003) and lamelliopodia of fibroblast (Watanabe and Mitchison, 2002).

The dynamic maintenance of spine structures explains why spines shrink and disappear in extreme conditions such as chilling (Kirov et al., 2004; Roelandse and Matus, 2004), strong stimulation (Hasbani et al., 2001) and anoxia (Jourdain et al., 2002), and why they rapidly reemerge after recovery to normal environments. The dynamic F-actin pool can also account for continuous spine motility, such as filopodia generation from spine heads (Fiala et al., 1998) and spine morphing (Fischer et al., 1998). It is conceivable that the dynamic organization of spine structures contributes in rapid structural alterations of spines during activity-dependent plasticity, which may be necessary for long-lasting modification of the entire synaptic structures.

It has been clarified that functional expression of AMPA receptors is dependent on F-actin, as it was blocked by latrunculin A (Kim and Lisman, 1999; Krucker et al., 2000). I have found that most F-actin in spine periphery is dynamic, indicating that AMPA receptors must be anchored to the dynamic pool

of F-actin. This is consistent with the fact that functional expression of AMPA receptors is proportional to spine-head volumes (Matsuzaki et al., 2001), since the amounts of the dynamic F-actin pool was proportional to spine-head volumes. Anchoring of AMPA receptors to the dynamic F-actin pool likely contributes in rapid alteration of functional AMPA receptor expression during LTP, which is accompanied with rapid actin-dependent spine enlargement (Matsuzaki et al., 2004).

### **Stable F-actin in spines**

I found that the stable F-actin pool was localized at the base of spine head, and turned over only slowly with a time constant (17 min) which is 15 times larger than that (1.2 min) of the dynamic pool. It is conceivable that the stable F-actin pool can act as a scaffold for dynamic F-actin to generate expansive force. If there might be no stable F-actin pool, the dynamic F-actin pool should have proceeded deep into dendritic shaft, and could not generate expansive force. Greater amounts of stable F-actin in larger spines may give a structural support for greater expansive force. I found that the stable F-actin pool often intruded into spine necks. Since thick necks were found only in large spines, it is conceivable that the larger stable pools and greater expansive forces of larger spines may induce thickening of spine necks. Thus, the stable F-actin pool may explain the spine head-neck relationship (Noguchi et al., 2005) – Large spines tend to have thick necks, if not always.

Moreover, I found that the amounts of the stable F-actin pool were proportional to the second power of spine-head volumes. This means that the

overall stability of F-actin is greater in larger spines, and that larger spines need to modify a disproportionately greater amount of the stable F-actin pool when they change their volumes during activity-dependent plasticity. This supra-linearity in the stability of F-actin might underlie resistance of larger spines for long-term enlargement (Matsuzaki et al., 2004), assuming that the alteration in the stable F-actin pool is the rate limiting step for the plasticity.

It will be therefore important to clarify how the stable F-actin pool is formed at the base of spine head and why it shows supra-linear dependence on spine volumes. It is conceivable that the flow of dynamic F-actin makes the stable F-actin pool localize at the base of spine head, and that resulting more distant localization of the stable pool from PSD contributes in the slower turnover rates of F-actin. More specifically, electron microscopic investigation of F-actin distribution using photoconversion of DAB with fluorescent phalloidin has demonstrated that dense labeling was found particularly around spine apparatus (Capani et al., 2001), which are preferentially localized at the base of spines with large spine heads (Spacek and Harris, 1997), in conformity with the localization of the stable F-actin pool. It has been reported that synaptopodin is an actin and  $\alpha$ -actinin binding protein, and localized in spine neck and close association with spine apparatus (Deller et al., 2000). The mice lacking synaptopodin is devoid of spine apparatus, and impaired in LTP (Deller et al., 2003). Thus, spine apparatus and associated molecules may, at least partly, account for the localization and amount of the stable F-actin pool. The stable F-actin pool may show some similarities with the actin arc of growth cone (Zhang et al., 2003), which is formed at the base of peripheral F-actin, and is more stable than the

peripheral F-actin. The actin arc is involved in growth cone collapse, and found to be regulated by Rho-GTPase (Zhang et al., 2003).

In summary, I have found that the segregated organizations of the two F-actin pools are essential for spine head and neck structures using two-photon photoactivation of PAGFP-actin. On the whole, F-actin in smaller spines is more dynamic, and may be susceptible to rapid structural plasticity, while F-actin in larger spines is more stable, and may contribute in long-term stability of excitatory synaptic transmission. Our approach will aid further clarification of molecular mechanisms of spine structures, functions and their plasticity.

## **Acknowledgments**

I'd like to extend my deepest thanks to Prof. Haruo Kasai (University of Tokyo) for continuous and valuable guidance, discussion, and encouragement throughout this research. Also, I'd like to express my sincere gratitude to Dr. Masanori Matsuzaki (University of Tokyo) for cooperation and helpful discussion throughout this research, Dr. Jun Noguchi (University of Tokyo), Dr. Takuya Kishimoto (University of Tokyo) and Dr. Tomomi Nemoto (National Institute for Physiological Sciences) for many helpful suggestions. I thank Mr. Naoki Takahashi, Ms. Tamaki Kise, and Ms. Tokiko Suzuki for excellent technical assistance, and Kasai laboratory members for helpful assistances and encouragements.

This work was supported by Grants-in-Aid from the Ministry of Education, Culture, Sports, Science, and Technology of Japan (H.K., M.M.) as well as by grants from the Human Frontier Science Program (H.K.), NIH (H.K.), the Takeda Science Foundation (H.K.). N.H. is a fellow of JSPS.

## References

Allison,D.W., Gelfand,V.I., Spector,I., and Craig,A.M. (1998). Role of actin in anchoring postsynaptic receptors in cultured hippocampal neurons: differential attachment of NMDA versus AMPA receptors. *J. Neurosci.* *18*, 2423-2436.

Capani,F., Martone,M.E., Deerinck,T.J., and Ellisman,M.H. (2001). Selective localization of high concentrations of F-actin in subpopulations of dendritic spines in rat central nervous system: a three-dimensional electron microscopic study. *J. Comp Neurol.* *435*, 156-170.

Crank,J. (1975). *The mathematics of diffusion* (Oxford: Oxford University Press).

Deller,T., Korte,M., Chabanis,S., Drakew,A., Schwegler,H., Stefani,G.G., Zuniga,A., Schwarz,K., Bonhoeffer,T., Zeller,R., Frotscher,M., and Mundel,P. (2003). Synaptopodin-deficient mice lack a spine apparatus and show deficits in synaptic plasticity. *Proc. Natl. Acad. Sci. U. S. A* *100*, 10494-10499.

Deller,T., Merten,T., Roth,S.U., Mundel,P., and Frotscher,M. (2000). Actin-associated protein synaptopodin in the rat hippocampal formation: localization in the spine neck and close association with the spine apparatus of principal neurons. *J Comp Neurol* *418*, 164-181.

El-Husseini,A.E., Schnell,E., Chetkovich,D.M., Nicoll,R.A., and Bredt,D.S. (2000). PSD-95 involvement in maturation of excitatory synapses. *Science* *1364-1368*.

Ethell,I.M., Irie,F., Kalo,M.S., Couchman,J.R., Pasquale,E.B., and Yamaguchi,Y. (2001). EphB/syndecan-2 signaling in dendritic spine morphogenesis. *Neuron* *31*, 1001-1013.

Fiala, J.C., Feinberg, M., Popov, V., and Harris, K.M. (1998). Synaptogenesis via dendritic filopodia in developing hippocampal area CA1. *J Neurosci* 18, 8900-8911.

Fifkova, E. (1985). Actin in the nervous system. *Brain Res.* 356, 187-215.

Fischer, M., Kaech, S., Knutti, D., and Matus, A. (1998). Rapid actin-based plasticity in dendritic spines. *Neuron* 20, 847-854.

Harris, K.M., and Stevens, J.K. (1989). Dendritic spines of CA 1 pyramidal cells in the rat hippocampus: serial electron microscopy with reference to their biophysical characteristics. *J. Neurosci.* 9, 2982-2997.

Hasbani, M.J., Schlieff, M.L., Fisher, D.A., and Goldberg, M.P. (2001). Dendritic spines lost during glutamate receptor activation reemerge at original sites of synaptic contact. *J. Neurosci.* 21, 2393-2403.

Hayashi, Y., and Majewska, A.K. (2005). Dendritic spine geometry: functional implication and regulation. *Neuron* 46, 529-532.

Hering, H., and Sheng, M. (2001). Dendritic spines: structure, dynamics and regulation. *Nat. Rev. Neurosci.* 2, 880-888.

Holtmaat, A.J., Trachtenberg, J.T., Wilbrecht, L., Shepherd, G.M., Zhang, X., Knott, G.W., and Svoboda, K. (2005). Transient and persistent dendritic spines in the neocortex in vivo. *Neuron* 45, 279-291.

Irie, F., and Yamaguchi, Y. (2002). EphB receptors regulate dendritic spine development via intersectin, Cdc42 and N-WASP. *Nat. Neurosci.* 5, 1117-1118.

- Jourdain,P., Nikonenko,I., Alberi,S., and Muller,D. (2002). Remodeling of hippocampal synaptic networks by a brief anoxia-hypoglycemia. *J. Neurosci.* 22, 3108-3116.
- Kim,C.H., and Lisman,J.E. (1999). A role of actin filament in synaptic transmission and long-term potentiation. *J. Neurosci.* 19, 4314-4324.
- Kirov,S.A., Petrak,L.J., Fiala,J.C., and Harris,K.M. (2004). Dendritic spines disappear with chilling but proliferate excessively upon rewarming of mature hippocampus. *Neuroscience* 127, 69-80.
- Korkotian,E., and Segal,M. (2001). Spike-associated fast contraction of dendritic spines in cultured hippocampal neurons. *Neuron* 30, 751-758.
- Krucker,T., Siggins,G.R., and Halpain,S. (2000). Dynamic actin filaments are required for stable long-term potentiation (LTP) in area CA1 of the hippocampus. *Proc. Natl. Acad. Sci. U. S. A* 97, 6856-6861.
- Matsuzaki,M., Ellis-Davies,G.C.R., Nemoto,T., Miyashita,Y., Iino,M., and Kasai,H. (2001). Dendritic spine geometry is critical for AMPA receptor expression in hippocampal CA1 pyramidal neurons. *Nat. Neurosci.* 4, 1086-1092.
- Matsuzaki,M., Honkura,N., Ellis-Davies,G.C., and Kasai,H. (2004). Structural basis of long-term potentiation in single dendritic spines. *Nature* 429, 761-766.
- Matus,A., Ackermann,M., Pehling,G., Byers,H.R., and Fujiwara,K. (1982). High actin concentrations in brain dendritic spines and postsynaptic densities. *Proc. Natl. Acad. Sci. U. S. A* 79, 7590-7594.

Mogilner,A., and Oster,G. (1996). Cell motility driven by actin polymerization. *Biophys. J.* 71, 3030-3045.

Noguchi,J., Matsuzaki,M., Ellis-Davies,G.C.R., and Kasai,H. (2005). Spine-neck geometry determines NMDA receptor-dependent  $Ca^{2+}$  signaling in dendrites. *Neuron* 46, 609-622.

Okamura,K., Tanaka,H., Yagita,Y., Saeki,Y., Taguchi,A., Hiraoka,Y., Zeng,L.H., Colman,D.R., and Miki,N. (2004). Cadherin activity is required for activity-induced spine remodeling. *J. Cell Biol.* 167, 961-972.

Pak,D.T., Yang,S., Rudolph-Correia,S., Kim,E., and Sheng,M. (2001). Regulation of dendritic spine morphology by SPAR, a PSD-95-associated RapGAP. *Neuron* 31, 289-303.

Patterson,G.H., and Lippincott-Schwartz,J. (2002). A photoactivatable GFP for selective photolabeling of proteins and cells. *Science* 297, 1873-1877.

Pollard,T.D., and Borisy,G.G. (2003). Cellular motility driven by assembly and disassembly of actin filaments. *Cell* 112, 453-465.

Roelandse,M., and Matus,A. (2004). Hypothermia-associated loss of dendritic spines. *J. Neurosci.* 24, 7843-7847.

Sala,C., Piech,V., Wilson,N.R., Passafaro,M., Liu,G., and Sheng,M. (2001). Regulation of dendritic spine morphology and synaptic function by Shank and Homer. *Neuron* 31, 115-130.

Schneider,M., Barozzi,S., Testa,I., Faretta,M., and Diaspro,A. (2005). Two-photon activation and excitation properties of PA-GFP in the 720-920-nm region. *Biophys. J.* 89, 1346-1352.

Spacek,J., and Harris,K.M. (1997). Three-dimensional organization of smooth endoplasmic reticulum in hippocampal CA1 dendrites and dendritic spines of the immature and mature rat. *J. Neurosci.* 17, 190-203.

Star,E.N., Kwiatkowski,D.J., and Murthy,V.N. (2002). Rapid turnover of actin in dendritic spines and its regulation by activity. *Nat. Neurosci.* 5, 239-246.

Swaminathan,R., Hoang,C.P., and Verkman,A.S. (1997). Photobleaching recovery and anisotropy decay of green fluorescent protein GFP-S65T in solution and cells: cytoplasmic viscosity probed by green fluorescent protein translational and rotational diffusion. *Biophys. J.* 72, 1900-1907.

Watanabe,N., and Mitchison,T.J. (2002). Single-molecule speckle analysis of actin filament turnover in lamellipodia. *Science* 295, 1083-1086.

Zhang,X.F., Schaefer,A.W., Burnette,D.T., Schoonderwoert,V.T., and Forscher,P. (2003). Rho-dependent contractile responses in the neuronal growth cone are independent of classical peripheral retrograde actin flow. *Neuron* 40, 931-944.

## Figure Legends

**Figure 1.** Rapid diffusion of PAGFP-actin along a dendritic shaft.

**(A-C)** Two-photon fluorescent images of a dendritic branch transfected both with mRFP (A) and PAGFP-actin (B,C). Excitation wavelengths are 960 nm and 710 nm for (A, C) and (B), respectively, and fluorescence was detected at 500-550 nm and 590-680 nm for (B,C) and (A), respectively. The images were obtained with three-dimensional reconstruction by image stacking. **(D)** A line-scan image of PA-GFP in the dendrite shown in (A), where a short pulse (1 ms) of photoactivation at 710 nm was applied at the red arrow. The line for imaging and the point for photoactivation were indicated by the green line and red point, respectively, in (A). **(E, F)** Time courses of PAGFP-actin fluorescence after photoactivation. The time axis is expanded in (F). The blue dashed lines indicate the linear fit of the decay curve more than 200 ms after photoactivation. **(G)** Spatial profile of PAGFP-actin fluorescence at various times after photoactivation. Smooth lines were Gaussian fittings of the profiles. **(H, I)** Variances of Gaussian distributions obtained as shown in (G) plotted against times after photoactivation. The line in (H) shows a linear fitting of the initial ( $\leq 10$  ms) part of the time course.

**Figure 2.** Diffusion out of PAGFP-actin from spine heads.

(A) An mRFP image of a single dendritic spine obtained from three-dimensional images. (B) A line scan image of PAGFP-actin along the green line depicted in (A). Photoactivation was effected at the time period indicated by the red bar. (C) Time course of PAGFP-actin fluorescence after photoactivation. The blue dashed line is a linear fit of the decay more than 1.5 s after photoactivation. (D) Concentrations of actins in the forms of G-actin and F-actin in dendritic shaft and spines by normalizing the total actin concentration in spine head as 1 (spine unit, s.u.). Data were obtained as indicated in the text from 7 dendritic shaft and 7 spine heads. Bars represent SDs.

**Figure 3.** Two pools of F-actin in spine heads studies with whole-spine activation of PAGFP-actin.

(A) An mRFP image of small and large dendritic spines, where regions of photoactivation and fluorescent measurement were depicted by red circles. The image was obtained from three-dimensional images. (B, C) Time courses of PAGFP-actin fluorescence after photoactivation of the regions indicated in (A) with two dimensional images acquired every 10 s. Dashed lines are linear fitting of the decay curve more than 2 min after photoactivation. (D) The fractions of the stable F-actin pool in spines with various head volumes. The linear regression line is shown. (E) Correlation between fluorescence of PAGFP-actin immediately after photoactivation and spine-head volumes of many spines in the same dendritic branch. The line shows a linear regression. (F) Double logarithmic plots of correlations between the fluorescence intensity of PAGFP-actin immediately after photoactivation and spine-head volumes obtained in the same dendrites. Different symbols represent data obtained from 6 dendrites.

**Figure 4.** Spatial distribution of the dynamic and stable F-actin pools in a spine visualized with whole-spine activation of PAGFP-actin.

**(A)** mRFP image of a spine where the region of photoactivation is indicated by a red circle. The scale represents the coordinate for fluorescence profiles shown in (D,E). **(B)** PAGFP-actin images after photoactivation. The color bar indicates pseudocolor cord of PAGFP-actin fluorescence. White lines indicate contours of the spine. **(C)** Predicted distributions of the dynamic and stable F-actin pools. The distribution of the stable pool (c2) was obtained by scaling the fluorescence image 300 s after photoactivation by 1.4 times to correct for the turnover during 300 s. The distribution of the dynamic pool (c1) was obtained by subtracting fluorescence image immediately after photoactivation (b1) with that of the stable pool (c2). **(D,E)** Spatial profiles of PAGFP-actin fluorescence along x-axis for the data shown in (B) and (C), respectively. Fluorescence intensities were averaged along y-axis over 1  $\mu\text{m}$ . All images were two dimensional scanning. Fluorescence intensities were averaged along y-axis for 1  $\mu\text{m}$ .

**Figure 5.** Direct visualization of F-actin flow in single spines with point photoactivation of PAGFP-actin.

**(A,B,C)** Images of mRFP and PAGFP-actin fluorescence in medium-sized spines with spine-head volume of  $0.15 \mu\text{m}^3$  (A) and in a large spine with spine-head volume of  $0.5 \mu\text{m}^3$  (B,C). The point of photoactivation is indicated by a red point in the mRFP image (a1,b1,c1). Fluorescence images of PAGFP-actin at various time points indicated in (a2-a4, b2-b4, c2-c4) after point photoactivation. Fluorescence intensity was pseudocolor coded as in Fig. 4, and white lines represent contours of spines. **(D,E,F)** Fluorescence profiles along x-axis indicated in (a1,b1,c1) at various times after the photoactivation. All images were two dimensional scanning. Fluorescence intensities were averaged along y-axis for  $1 \mu\text{m}$ .

**Figure 6.** Distribution of the stable pool of F-actin in various spines labeled with point photoactivation.

(A) mRFP fluorescence images of various spines with head volumes of  $0.5 \mu\text{m}^3$ ,  $0.15 \mu\text{m}^3$ ,  $0.3 \mu\text{m}^3$ ,  $0.2 \mu\text{m}^3$  and  $0.35 \mu\text{m}^3$ , respectively. (B) Fluorescence images of PAGFP-actin 60 s after point photoactivation at the base of the spines shown in (A). Fluorescence of PAGFP-actin is pseudocolor coded as shown in Fig. 4. White lines represent contours of spines. (C) The fractions of stable F-actin obtained as shown in Fig. 3D, except that photoactivation was induced at a single point at the base of spines. All images were obtained by two dimensional scanning.

**Figure 7.** Quantitative analysis of the F-actin flow in the dynamic pool.

**(A, B)** Time courses of the mean x-positions of PAGFP-actin fluorescence in a medium-sized spine (A) and in a large spine (B) shown in Fig. 5A and B, respectively. **(C,D)** Spine-head volume dependences of the maximal speeds (C) and lengths (D) of the actin flow obtained from the maximal slope and position, respectively, of the plots shown in (A,B). **(E)** Time courses of decay in PAGFP-actin fluorescence after a point photoactivation at the tip of medium-sized (black) and large spines (red). **(F)** Time constants of the decay obtained as shown in (E) plotted against spine-head volumes in many spines.

**Figure 8.** Effects of latrunculin A on spine shapes and actin distributions.

**(A)** Images of mRFP1 and Venus-actin in a dendritic branch treated with Lat A at 10  $\mu$ M for 10 min. Images were obtained by three-dimensional reconstruction by image stacking. **(B)** The time courses of fluorescence of mRFP1 and Venus-actin in a spine indicated by the arrow in (A). **(C)** Relationship between spine-head volumes before and after Lat A treatment in many spines at 10 min after Lat A treatment.

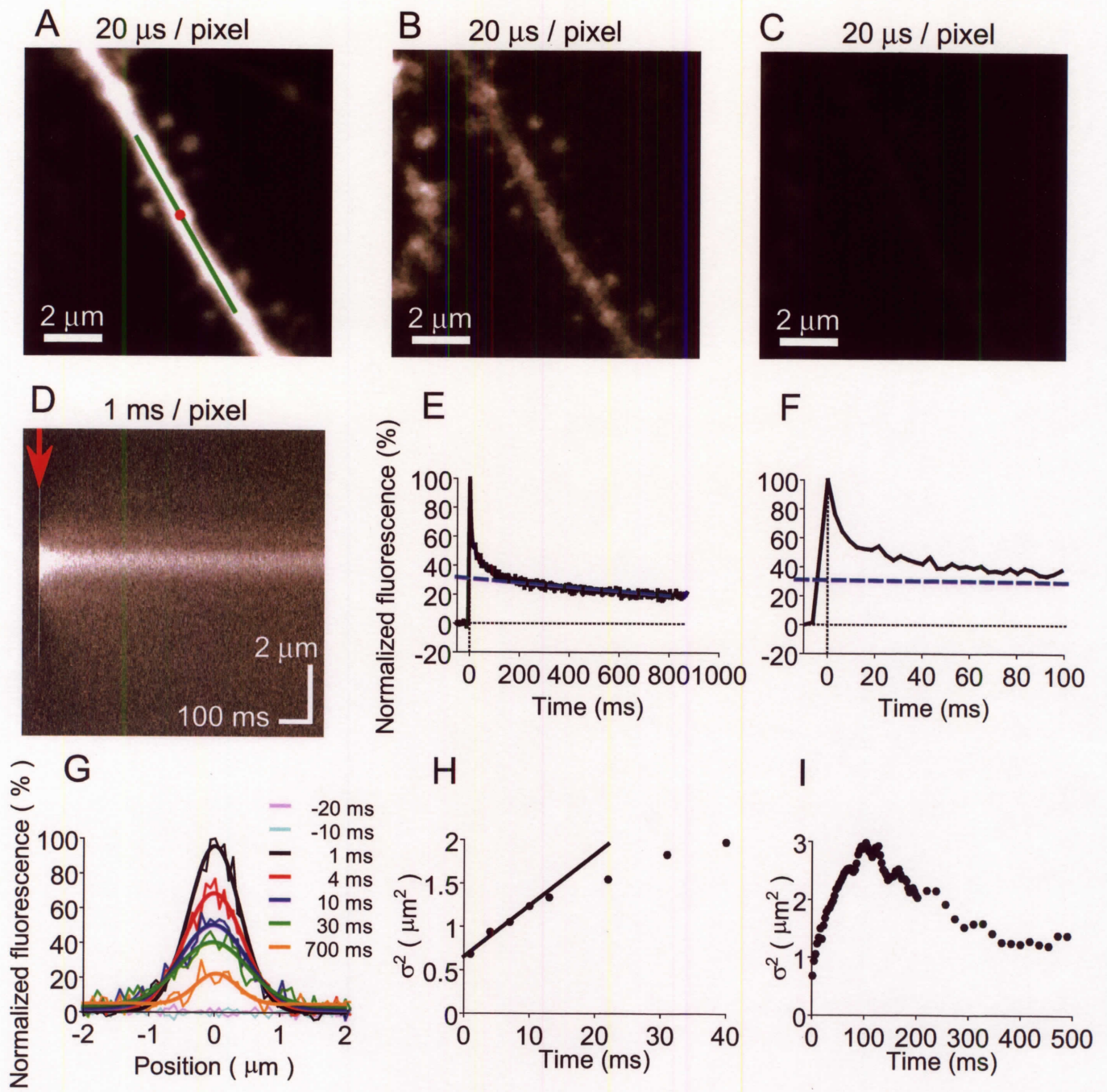


Figure 1

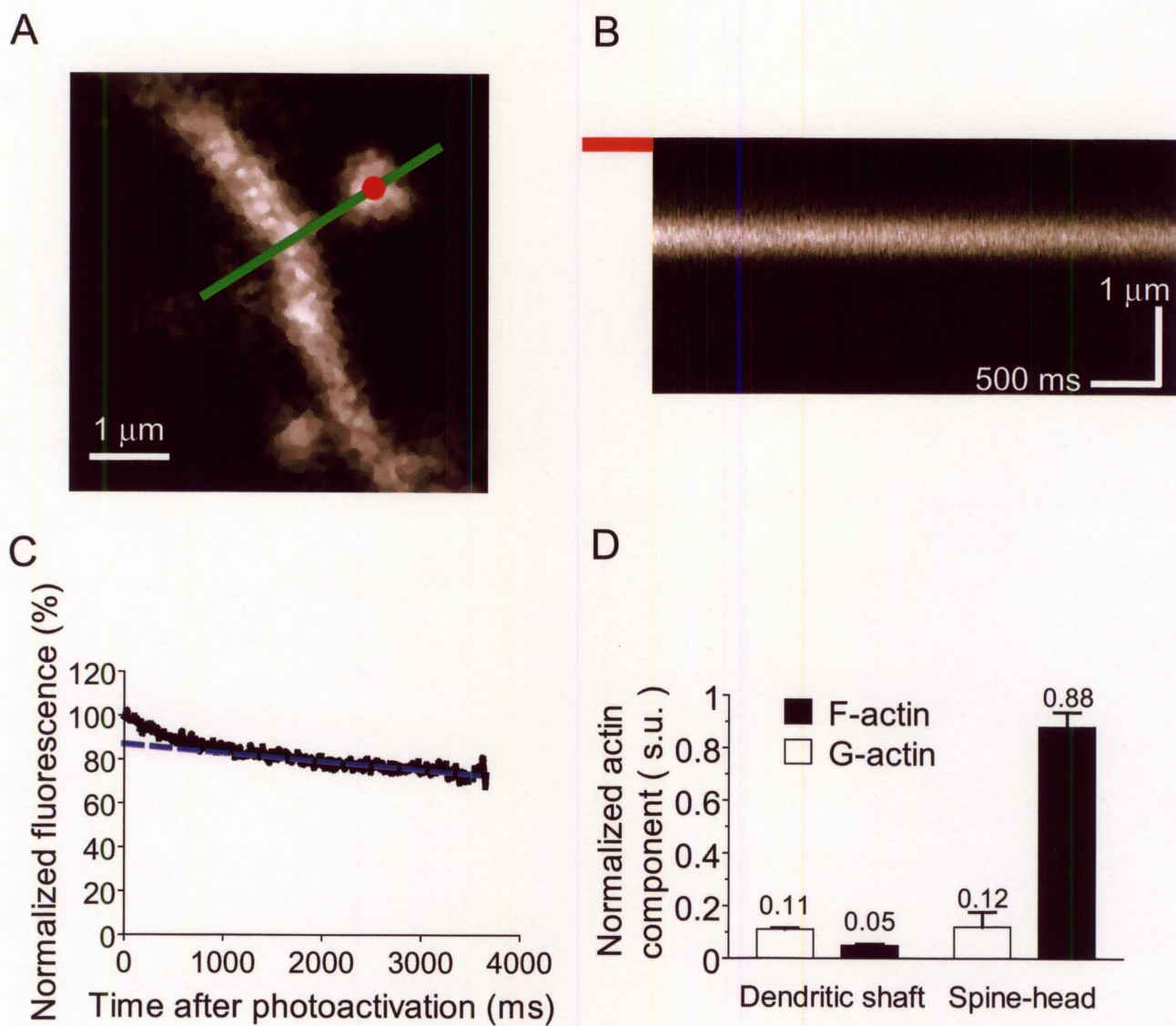


Figure 2

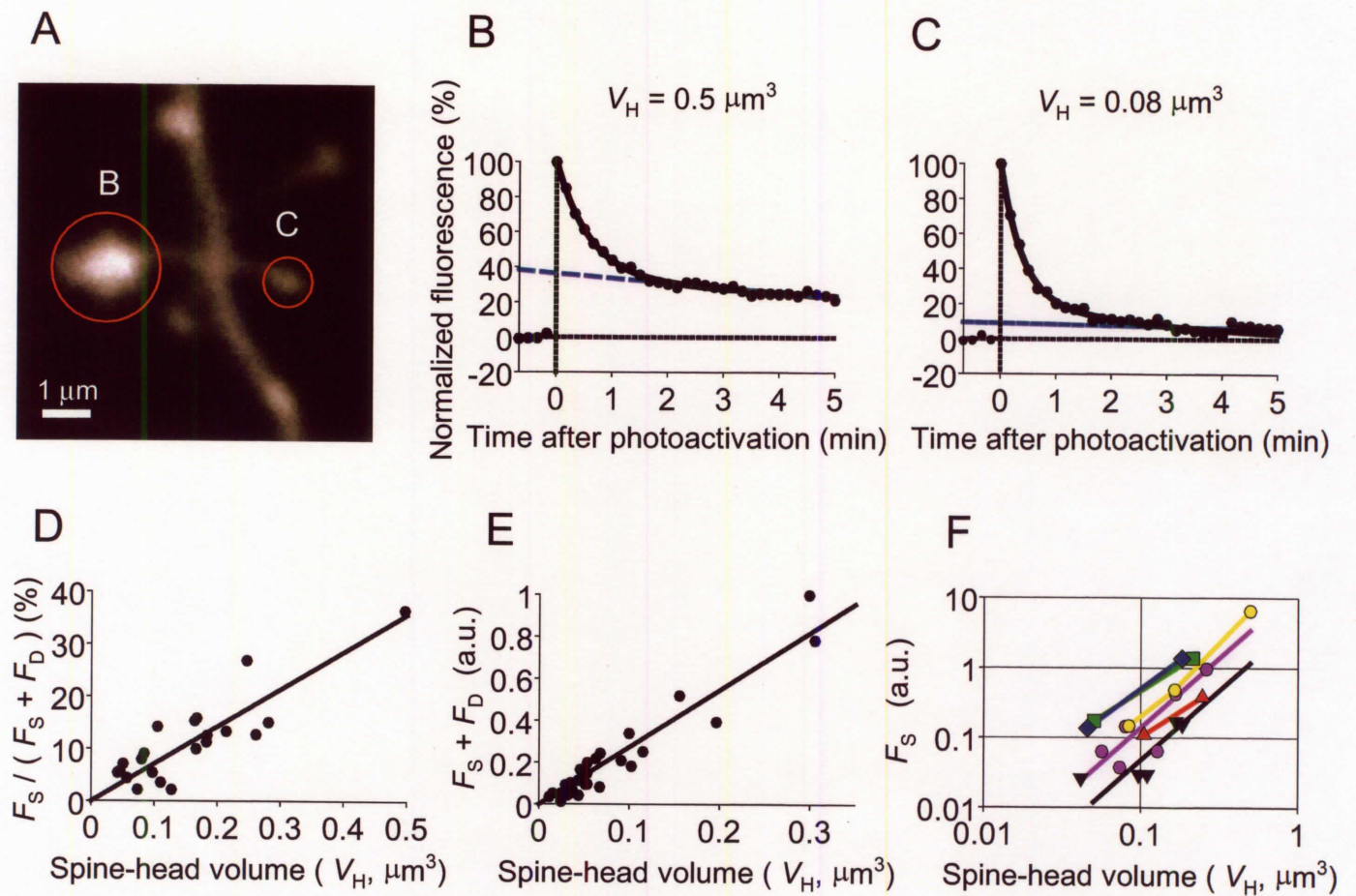


Figure 3

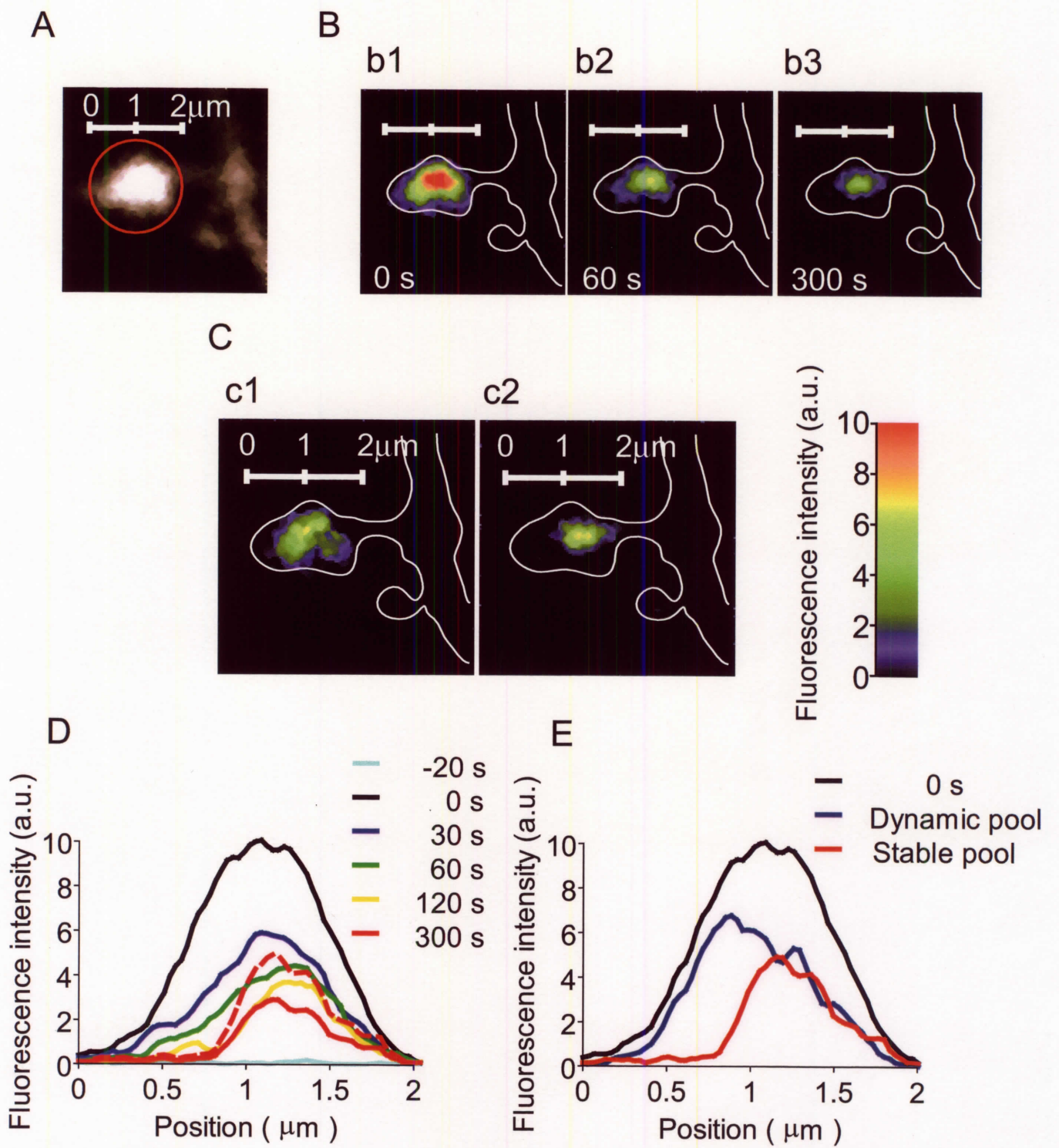


Figure 4

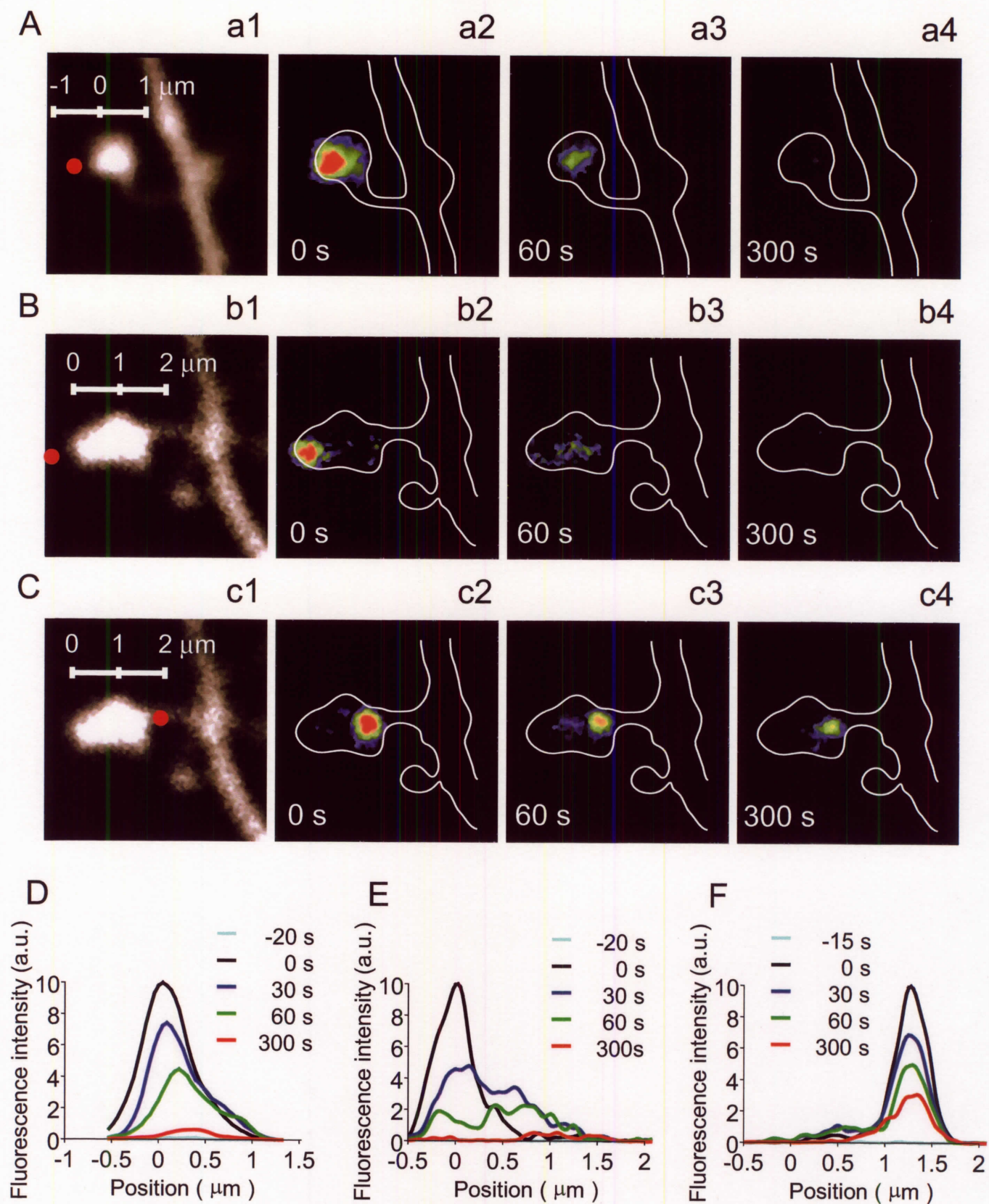


Figure 5

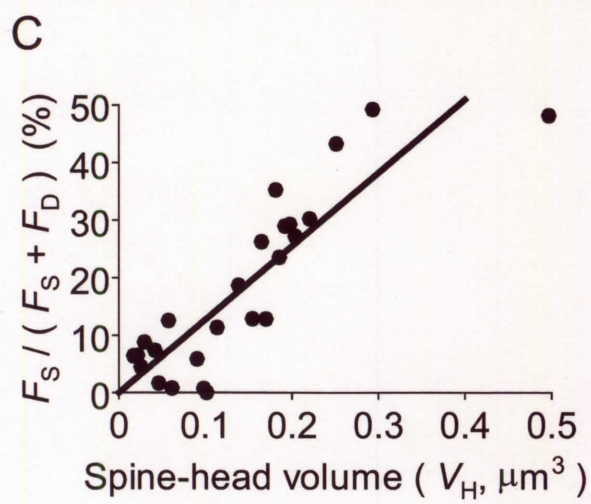
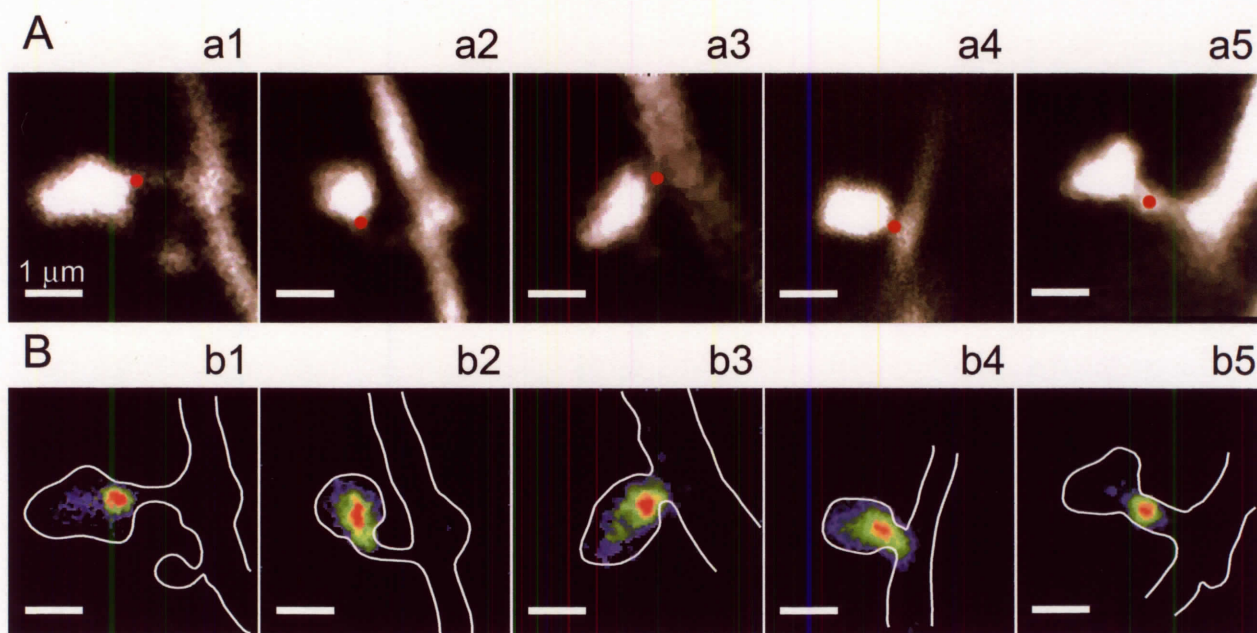


Figure 6

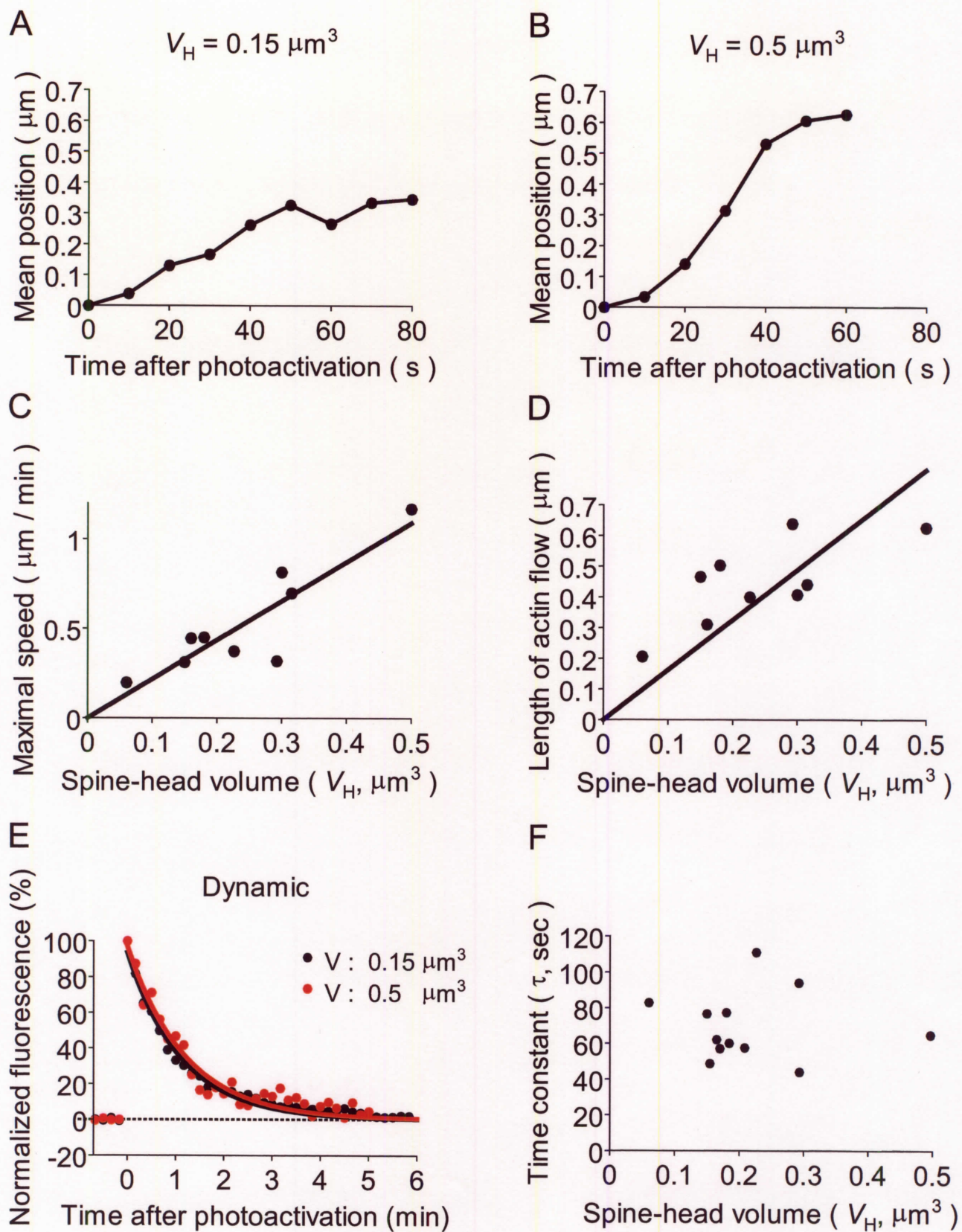


Figure 7

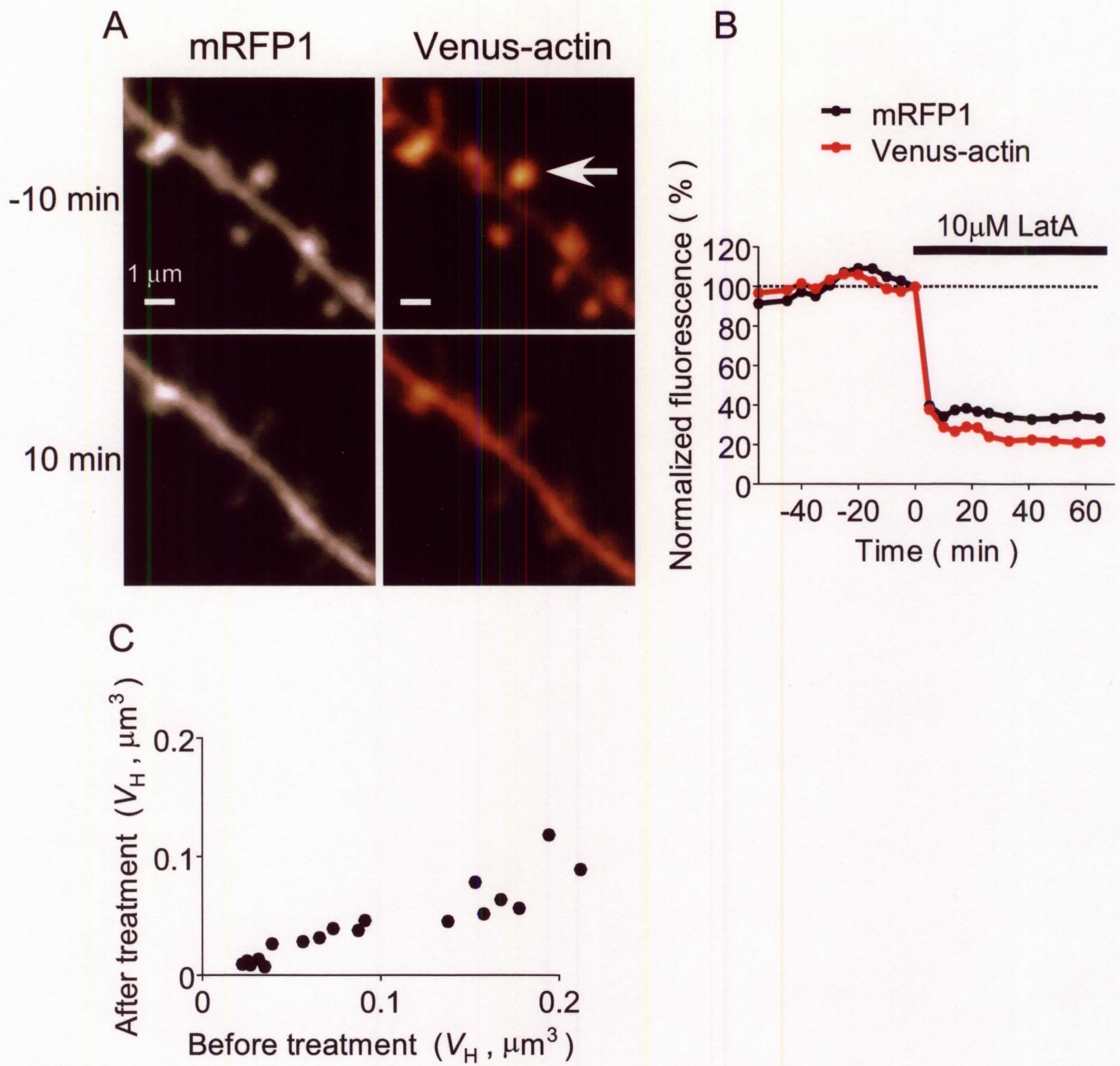


Figure 8